

A new prediction model for mining subsidence deformation: the arc tangent function model

Lei Nie · Hongfei Wang · Yan Xu · Zechuang Li

Received: 2 July 2014 / Accepted: 4 September 2014 / Published online: 12 September 2014
© Springer Science+Business Media Dordrecht 2014

Abstract Ground subsidence in underground coal mining areas causes environmental damage and creates hazards on the ground surface, which is long-term, widely distributed, and can lead to large-scale geological disasters. Achieving a high-precision method to predict mining subsidence deformation is very important for assessing environmental damage and countermeasures. In this paper, based on the “S”-type settlement curves of the monitoring points in the collapsed pit and the failure mechanism of rock strata on the goaf, the arc tangent function model was proposed and applied to the Taihe coal mine in Fushun, Liaoning Province, China. Using the Levenberg–Marquardt algorithm for nonlinear curve fitting of the data, the parameters of the model are obtained, and extending it in time, the prediction function will be obtained. Using different monitoring data to validate the model shows that the accuracy of the medium- and short-term forecasting is very good. With continuous updating of the monitoring data, the forecasting achieves higher accuracy and the function of dynamic track forecasting is achieved. A very high correlation coefficient was obtained (0.996) using all the available data from the monitoring point for the best-fit curve. This prediction model provides a reference for the evaluation and treatment of ground subsidence in the Taihe coal mining area.

Keywords Ground subsidence · Geological disasters · Arc tangent function · “S”-type settlement curve · Dynamic track forecasting

1 Introduction

In recent years, with China’s urban expansion and modernization, the demand for mineral resources has led to intensive growth of underground mining of these resources. Along with underground mining, ground subsidence disasters are a common occurrence.

L. Nie · H. Wang (✉) · Y. Xu · Z. Li
Jilin University, Changchun, Jilin, China
e-mail: whf001988@126.com

According to data from the China Geological Environment Bulletin, the number of surface subsidence hazards was 316 in 2009, 499 in 2010, and 360 in 2011 (Nie et al. 2013). Ground subsidence leads to various forms of damage such as that to buildings, drainage systems, and roads (Williams et al. 1998). Geological disasters resulting from ground subsidence restrict the development of mining cities and cause huge economic losses in China every year. The wide distributions, long durations, and intensities of the damage of ground subsidence have attracted much attention. Researching the ground subsidence characteristics caused by underground mining and accurately predicting the deformation caused by ground subsidence is one of the most important aspects for evaluation and treatment of ground subsidence in mining areas.

Various methods have been suggested for the prediction of subsidence caused by underground mining. Saro et al. (2012) studied the spatial prediction of ground subsidence susceptibility (GSS) around abandoned coal mines in Jeong-am, Gangwon-do, South Korea using the artificial neural network (ANN) and geographic information system approaches. FLAC3D is a 3-D finite difference computer program for solving rock and soil mechanics problems. Nie et al. (2013) and Xu et al. (2013) used FLAC3D to conduct numerical simulation of rock movement caused by coal mining. Saeidi et al. (2013) developed a methodology and an algorithm based on the traditional influence function method that considered the different influence angles. In the area of deep mining subsidence prediction and monitoring, Wang et al. (2011) introduced a dynamic prediction method that combines the probability-integral method with the differential interferometric synthetic aperture radar (D-InSAR) measuring technique. Li et al. (2013) used probability integration and numerical simulation, the most commonly used methods in movement and deformation prediction, to compute ground subsidence deformation based on real measurement data. By comparing the final subsidence graphs obtained by the two methods with the actual data, they evaluated the applicability and accuracy of the two methods.

Ground subsidence is caused by internal and external geological forces acting on the earth's crustal surfaces. Its generation mechanism is complex and volatile (Xu et al. 2014). Most of the existing methods for modeling ground subsidence consider the characteristics of the geological environment of the mine and the interaction between the factors influencing the subsidence; however, obtaining the prediction model parameters is difficult. Hence, these methods have a limited scope of application for predicting subsidence and deformation in mining areas. Real-time monitoring of ground subsidence deformation provides important data for researchers. In China, extensive ground subsidence monitoring data have been acquired. These data can be collated to extract information about the deformation of the mining subsidence. Based on this information, a model to predict the trends of the ground subsidence deformation can be obtained.

Combined with the "S"-type settlement curve of monitoring point G22 at a collapsed pit in the Taihe coal mine in Fushun, Liaoning Province, China, and the "S"-type deformation characteristics of rock mass from different fracture zones in the overlying strata of the goaf, the arc tangent function model was proposed. The parameters of the model are obtained through using the "Levenberg–Marquard" algorithm for nonlinear curve fitting of the monitoring data, and then, the prediction function is achieved. Unlike models based on the physical equations of ground deformation, this model is based directly on observations and field data. There is no need to consider the specific characteristics of the mine geological environment or the interaction between the factors affecting the mining subsidence. Using different data from monitoring point G22 for model validation, we demonstrated the good medium- and short-term forecasting ability of the model. Continuous updating of the monitoring data increases the accuracy of the forecast and

achieves dynamic track forecasting. The high precision of this prediction model provides a reference for the evaluation and treatment of ground subsidence of geological disasters in the Taihe coal mining area.

2 Study area and monitoring data

The Fushun Taihe coal mine is located in the eastern part of Fushun in Liaoning Province, China (Fig. 1). The shape of the mining area is an irregular polygon. The length of the area from east to west is 1.845 km, and the width from north to south is 1.567 km. The area is about 1.6448 km² (Fig. 2). The eastern and southern parts of the mining area are the original Longfeng coal mine goaf, the western part is the Laohutai mine, and to the north is the Hunhe River. Mining at the Taihe coal mining continues on the basis of the original Longfeng coal mine at an elevation of -50 to -570 m. The dip angle of the coal seam varies from 10 to 25°. The average coal thickness in the mining area is 24.35 m, with a maximum of 45.70 m and a minimum of 0.60 m, thinning gradually from west to east. Taihe coal mine conducts its slice mining by using blasting and caving technology. Hanging beam hydraulic stents are used to support the roof in the working face.

The strata from the top of the mining goaf to the ground surface can be divided into three layers: the oil shale layer, mudstone layer, and quaternary alluvium. The coal seam roof is composed of oil shale, which is hard, dense, with well-developed joints, prone to collapse, and with low permeability. It is 90–120 m thick, with an average thickness of 95 m. The mudstone layer is composed of green block mudstone, 137–600 m thick with an average thickness of 460 m. The bottom of the quaternary alluvium is composed of conglomerate and sandy conglomerate, while the top of the quaternary alluvium is clay. The quaternary alluvium is 3–15 m thick with an average thickness of 12 m.

The deep geological structure is rather complex, with three faults, F13, F16, and F18 as shown in Fig. 2. F13 and F16 are normal faults located in the north of the mining field. F13 tends south with a dip angle ranging from 67 to 82°, making up the northern border of the mining field. F16 tends 320° with a dip angle of 28 to 72°. F18 is a reverse fault, tending 320–360° with a dip angle ranging from 45 to 60°.

The Taihe mine began coal production in 2010. To understand the impact of the coal mining on the ground deformation, six monitoring points were set up in the mining area and data were collected from December 9, 2010, until March 16, 2014. During the mining of Taihe coal, ground subsidence occurred along the Haixin road in the northeast part of the mining area over an area of 0.24 km² (Fig. 2). The maximum collapse depth was 2.1 m. Owing to the ground subsidence, the low-lying area is prone to flooding. The Haixin road had been repaired several times to raise the height of the roadbed. At present, houses on both sides of the road are under water (Fig. 2). The data from monitoring point G22 in the collapsed pit are shown in Table 1.

There were a total of 25 observations at the G22 monitoring point. The first day of monitoring was December 9, 2010, and the initial cumulative settlement value was set to 0. The curves showing the settlement measured at this monitoring point with time are shown in Fig. 3.

Geological processes such as land subsidence are composed of four phases, namely the initial, accelerating, decelerating, and end phases (Wang 2003). An “S”-type curve can reflect the characteristics of the various stages of the process. An appropriate “S”-type curve model can describe the subsidence process completely and predict the development trend of the deformation.

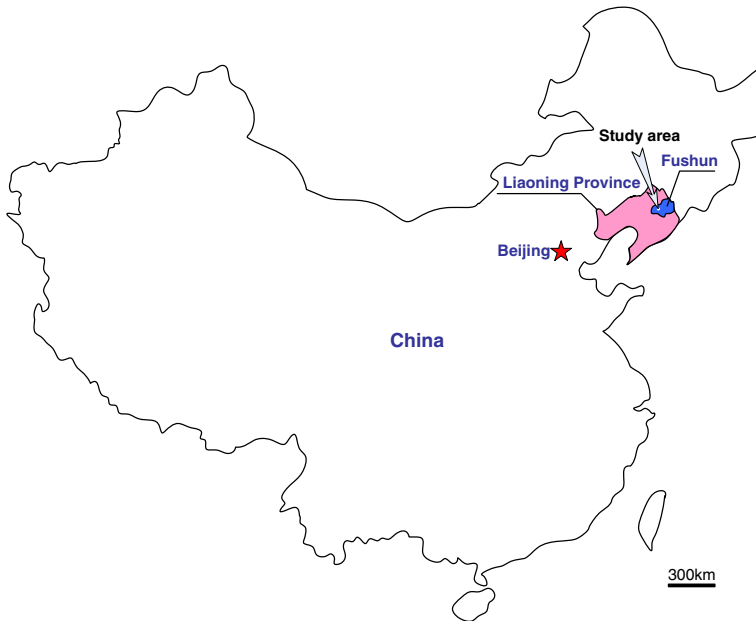


Fig. 1 Position of the study area

The deformation curve characteristics recorded at monitoring point G22 show that the mining subsidence deformation is generally composed of the acceleration stage and deceleration stage, typical of an “S”-type curve.

3 “S”-type settlement deformation characteristics of the rock mass in the goaf overburden damage zones

Generally, when the mining distance is equal to $1/4H$ – $1/2H$ (where H is the average mining depth), the effect of the mining spreads to the surface, causing ground subsidence. As mining activity continues, the free face of the overlying strata in the mined-out area increases. The deformation of the surrounding rock moves toward the mined-out area constantly. When the rock mass stress above the coal seam reaches its threshold value, it generates cracks or shear displacement, damaging the rock mass. The damaged rock mass under the action of gravity and the overburden pressure will fall down, piling up in the mined-out area, forming a caving zone. Rock mass with weak structural elements such as joints and cracks is most susceptible. When the gravity force in the rock mass above the caving zone exceeds the strength of the rock, it may lead to cracks, abscission layers, and fractures. The original rock layer formation is maintained; this rock mass forms the fracture zone. The rock mass above the fracture zone, under its own gravity and the weight of the overlying strata, tends to bend along the fracture zone, but will not rupture or fall off. Therefore, this zone is called the “bending zone.” The rock stratum from the coal seam roof to the ground is divided into three damage zones according to the extent of the voids, cracks, and the degree of damage to the overburden rock: the caving zone, the fracture

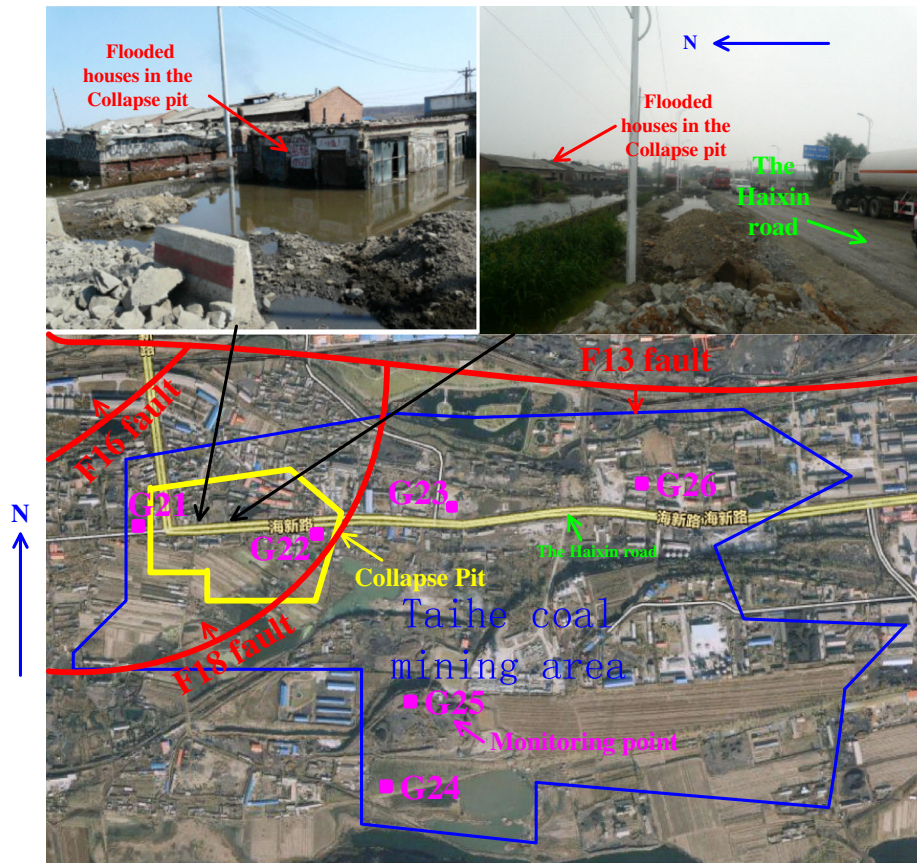


Fig. 2 Present characteristics in the study area

zone, and the bending zone (containing the Quaternary loose layer) (Zhao et al. 2010). The structure of the damage zones is shown in Fig. 4.

The process of stress redistribution leads to rock mass deformation; the deformation is composed of five stages: elastic deformation, plastic deformation, fragmentation, collapse, and compaction settlement. Owing to the high stiffness of the rock mass and the relatively small amount of elastic and plastic deformation, the mining subsidence deformation mainly consists of the fragmentation, collapse, and compaction settlement stages.

The main characteristics of the rock mass deformation in the caving zone can be described as follows. After some overlying strata in the mined-out area falls off, an area of accumulated fallen rock will form at the bottom of the goaf and a new mined-out area will form above the caving zone. With time, owing to gravity and the pressure of the rock mass above it, the overlying strata in the new mined-out area will distort and crack and then drop on top of the old fallen roof. This deformation feature will gradually shift upward from the original coal seam roof. Owing to the expansion of the rock mass, when the scale of the falling roof expands to a certain degree, the mined-out area will be filled with broken fallen rock. In the caving zone, the distance of the collapse of the rock mass from the bottom up becomes gradually smaller, and the deformation of the collapse stage also decreases. The

Table 1 Monitoring data of the monitoring point G22

Date (year/month/day)	Monitoring time t/day	The cumulative settlement deformation δ/cm
2010/12/9	1	0.00
2012/5/8	517	5.48
2012/5/19	528	5.72
2012/5/29	538	6.05
2012/6/21	561	6.94
2012/7/11	581	8.00
2012/7/23	593	8.39
2012/8/5	606	11.00
2012/8/26	627	12.92
2012/9/10	642	13.64
2012/9/28	660	14.17
2012/10/8	670	15.69
2012/11/8	701	16.76
2012/12/16	739	17.95
2013/1/19	773	19.86
2013/2/5	790	22.24
2013/2/24	809	23.26
2013/3/12	825	24.59
2013/5/10	884	25.85
2013/7/12	947	26.86
2013/9/15	1,012	27.30
2013/11/5	1,062	27.60
2013/12/24	1,112	27.71
2014/2/10	1,160	28.05
2014/3/16	1,194	28.26

collapse stage is an instantaneous deformation process, and the moment when it reaches its maximum speed corresponds to the inflection point in the “S” deformation curve; the tangent slope at the inflection point gradually decreases from the bottom of the caving zone to the top. With the continuous cracking and breaking of the overlying rock mass, the vertical stress of the fractured rock mass in the caving zone increases and the compaction settlement deformation increases with the height of the caving zone. According to the fractured rock compaction test (Su et al. 2012), the stress–strain curve can be described by $\varepsilon = b \ln a\sigma$. When the stress of the rock mass in the fracture zone and bending zone is transmitted to the caving zone, the vertical stress of the broken fallen rock mass in the caving zone reaches its maximum value. With time, the stress of the fractured rock mass in the caving zone reaches its maximum value and the compaction settlement gradually stabilizes. In the “S” deformation curve, this deformation phase corresponds to the part after the inflection point.

The main deformation characteristic of the rock mass in the fracture zone can be described as follows. The collapse stage disappears. Under the support of the caving zone, its own weight, and the pressure of the rock mass in the bending zone, the rock mass in the fracture zone begins its deformation. Because the compaction settlement of the rock mass

Fig. 3 Settlement deformation curve of the monitoring point G22

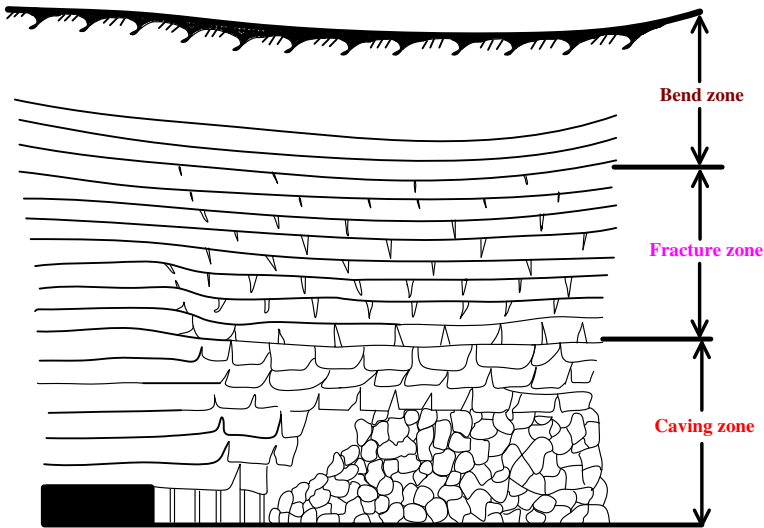
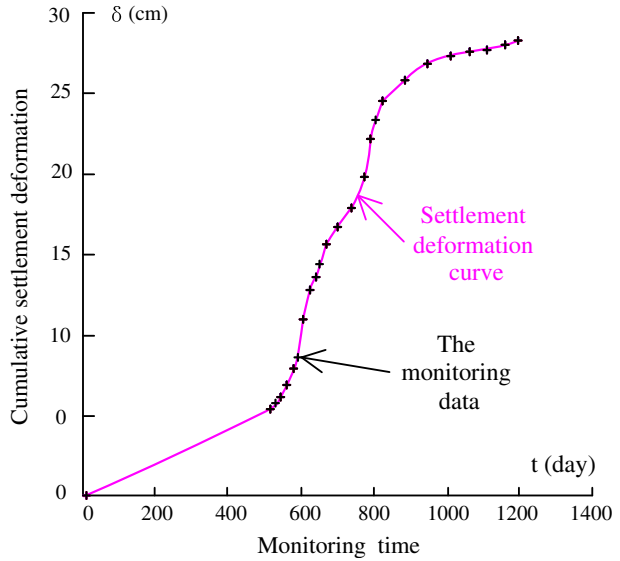


Fig. 4 Distribution chart of the caving zone, fracture zone, and bend zone (Zhao et al. 2010)

in the caving zone provides some deformation space for the rock mass in the fracture zone, the deformation of the rock mass in the fracture zone is accompanied by compaction settlement of the rock mass in the caving zone. Thus, settlement deformation of the rock mass in the fracture zone consists of two stages: shear displacement caused by the damage to the rock mass in the fracture zone (corresponding to the curve before the inflection point in the “S” deformation curve) and settlement deformation along with the compaction settlement of the lower fractured rock mass (corresponding to the curve after the inflection point in the “S” deformation curve).

The main deformation characteristics of the rock mass in the bending zone can be described as follows. The fragmentation stage and the collapse stage disappear. Under the support of the fracture zone and the action of its own weight, the rock mass in the bending zone begins its deformation along with the fracture zone. The deformation consists mainly of compaction settlement deformation. This stage contains accelerated subsidence (corresponding to the curve before the inflection point in the “S” deformation curve) and decelerated subsidence (corresponding to the curve after the inflection point in the “S” deformation curve). Accelerated subsidence occurs along the shear displacement caused by the damage of the rock mass in the fracture zone; decelerated subsidence occurs along the compaction settlement in the fracture zone.

The deformation characteristics of these three damaged zones are correlated; the “S”-type settlement deformation characteristics of the caving zone are transferred upward to the bending zone (Fig. 5), showing a lag in time and continuity in space. t_1 , t_2 , and t_3 are the times corresponding to the inflection points of the settlement deformation curve in the caving zone, fracture zone, and bending zone, respectively. δ_1 , δ_2 , and δ_3 represent the cumulative settlement deformation corresponding to the asymptotes of the curves. Figure 5 shows that $t_1 < t_2 < t_3$ and $\delta_1 > \delta_2 > \delta_3$. The settlement deformation features of the ground caused by the underground mining gradually transform from bending rock mass deformation characteristics to caving rock mass deformation characteristics when wide-range mining occurs at shallow depth and the overlying strata is poor.

4 The arc tangent function model

This function model is based on data of ground surface settlement that reflects the interaction of various factors affecting the subsidence deformation in the mining area. The data represent the overall characteristics of the ground deformation, and the model was derived by finding the function that best fits the ground settlement data. Through the analysis of surveillance data of monitoring point G22 and the settlement characteristics of the rock mass of different fracture zones in the mined-out area, the arc tangent function model was proposed, namely the “S”-type curve model. The model parameters are obtained by applying the Levenberg–Marquardt algorithm (Levenberg 1944; Marquardt 1963; Lourakis 2005) to find the nonlinear curve that best fit the ground settlement data. The proposed arc tangent function model, which describes an “S”-type curve, is

$$\delta = p_1 \{ \tan^{-1} p_0(t - p_2) + \tan^{-1} p_0 p_2 \} \quad (1)$$

where δ is the accumulative settlement value (cm), t is the monitoring time (days), and P_0 , P_1 , P_2 are coefficients that vary with the changes of the monitoring data.

Based on the development trend of the acquired deformation curve, the deformation trends at the monitoring points can be predicted, and the final settlement deformation value and the forecast function will be achieved.

The model prediction principle: in the model, when t tends to infinity, $\tan^{-1} p_0(t - p_2)$ reaches $\pm\pi/2$, and the curve is close to the asymptote $\delta = p_1(\pm\pi/2 + \tan^{-1} p_0 p_2)$. The asymptote value is the final settlement deformation value of the monitoring point. The correlation coefficient is used to evaluate the degree of correlation between the two variables, and the precision of the curve fitting. The correlation coefficient is

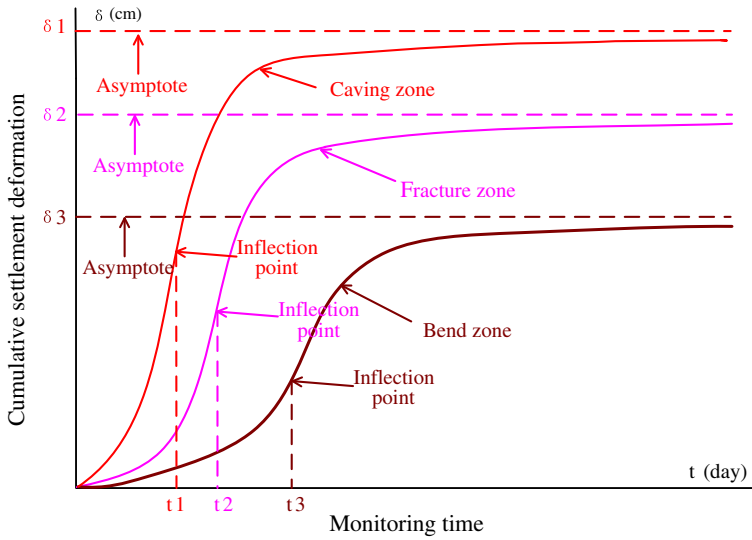


Fig. 5 Settlement deformation characteristics of the rock mass in the goaf overburden damage zones

$$R = \frac{\sum_{i=1}^n (t_i - \bar{t})(\delta_i - \bar{\delta})}{\sqrt{\sum_{i=1}^n (t_i - \bar{t})^2 \sum_{i=1}^n (\delta_i - \bar{\delta})^2}}$$

The arc tangent function model is set up on the basis that the deformation features of the ground subsidence are in accordance with “S”-shaped curve characteristics. So it has certain scope of application. This model will gain a better prediction effect when the overlying strata in the mined-out area under the action of its self-weight and the upper load. However, when large-scale external geological agency occurs, like earthquake, tectonic movement, the deformation features of the ground subsidence will be not in accordance with “S”-shaped curve characteristics. In this condition, the prediction precision will be low, and the model will be not suitable.

5 Model parameters and mathematical characteristics

P_0 represents the speed at which the deformation curve approaches the asymptote; the greater the absolute value of P_0 , the more rapidly the deformation curve approaches the asymptote. In other words, the time required for the settlement deformation of the monitoring point to stabilize will be shorter. P_1 represents the size of the asymptote numerical; the larger the absolute value of the asymptote of the deformation curve, the greater the final deformation settlement. P_2 corresponds to the inflection point of time (days) on the deformation curve, which represents the time of maximum settling velocity at the monitoring point.

The model function is a monotonically increasing function. When $t < P_2$, the acceleration is >0 , the tangent slope increases, the deformation curve is concave upward, and the deformation is in the acceleration phase. At $t = P_2$, the slope of the tangent reaches its maximum value. When $t > P_2$, the acceleration is <0 , the slope of the tangent

Table 2 Fitting results through adopting the previous 18, 20, 22, and 24 data items of monitoring point G22

The number of data items adopted	p_0	p_1	p_2	Residual error	Average residual error	Correlation coefficient
18	-0.0077	-10.11	655	12.96	0.72	0.992
20	-0.0070	-10.83	670	13.99	0.70	0.994
22	-0.0071	-10.72	668	14.07	0.64	0.995
24	-0.0072	-10.61	665	14.29	0.60	0.996

decreases, the deformation curve is convex downward, and the deformation is in the decelerating phase. When $t \rightarrow \infty$, the tangent slope is close to 0 and the deformation curve approaches a horizontal asymptote.

6 Model verification

To verify the accuracy of the model predictions, the previous 18, 20, 22, and 24 data items of monitoring point G22 were adopted to fit the model (Eq. (1)). The results are shown in Table 2. Residual error refers to the square sum of the differences between the measured values and predicted values in this table.

As the number of data items used in the calculation increased, the correlation between the curve and the data also increased. The correlation coefficient was above 0.99, indicating very high fitting precision. Using the model parameters obtained by the curve fitting, the predicted subsidence values for time t would be obtained. A comparison of the measured values with the predicted values (Table 3) shows that the error between the predicted value and measured value is smaller and the prediction accuracy is higher as the number of data items used in the fitting increases. With the increase of the fitting data, the measurement error of individual monitoring data will have less influence on the fitting accuracy. In addition, with the change of the mining conditions, the development trend of the ground subsidence is reflected on the monitoring data. Along with the continuous renewal of the data, the dynamic development trend of subsidence deformation in the mining area will be grasped and dynamic track forecasting can be achieved. For example, using the data taken before February 10, 2014, to forecast the subsidence on March 16, 2014, the forecast error is only 0.69 %, showing the very good short-term forecasting ability of the model. Using data recorded before March 12, 2013, to predict the settlement deformation of the following year, the error is still <5 % indicating that the accuracy of this model for medium-term forecasting is also very high. Despite the decrease in prediction accuracy as the forecast period increases, the model still provides good long-term forecast results.

7 Prediction models

To predict the final settlement deformation of monitoring point G22, all the data items from December 9, 2010, to March 16, 2014, were used to fit the model (Eq. (1)) and the model parameters P_0 , P_1 , and P_2 were obtained. The results are presented in Table 4, and the displacement versus time fitting curve is shown in Fig. 6.

Table 3 Comparison of the measured values with the predicted values when adopting the previous 18, 20, 22, and 24 data items of the monitoring point G22

Date (year/ month/ day)	Adopt the previous 18 data items		Adopt the previous 20 data items		Adopt the previous 22 data items		Adopt the previous 24 data items		
	Measured value (cm)	Predictive value (cm)	The error percentage between predictive value and measured value (%)	Predictive value (cm)	The error percentage between predictive value and measured value (%)	Predictive value (cm)	The error percentage between predictive value and measured value (%)	Predictive value (cm)	The error percentage between predictive value and measured value (%)
2013/5/10	25.85	24.56	5.00						
2013/7/12	26.86	25.54	4.90						
2013/9/15	27.30	26.25	3.85	27.45	0.56				
2013/11/5	27.60	26.65	3.43	27.95	1.28				
2013/12/24	27.71	26.98	2.65	28.35	2.32	28.17	1.67		
2014/2/10	28.05	27.23	2.92	28.66	2.19	28.48	1.52		
2014/3/16	28.26	27.38	3.10	28.85	2.10	28.66	1.42	28.45	0.69

Table 4 Fitting results of the monitoring point G22

The number of data items adopted	p_0	p_1	p_2	Residual error	Average residual error	Correlation coefficient
25	-0.0073	-10.59	655	14.32	0.57	0.996

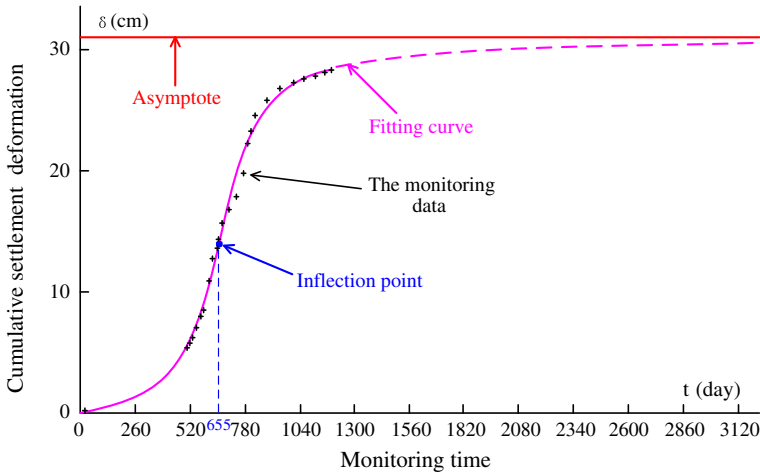


Fig. 6 Displacement versus time fitting curve of monitoring point G22

The expression of the settlement deformation can now be written as

$$\delta = -10.59 \times [\tan^{-1}[-0.0073 \times (t - 655)] - 1.36]$$

And the velocity v and acceleration a are

$$v = \frac{0.0773}{1 + [-0.0073 \times (t - 655)]^2}$$

$$a = \frac{-0.000008 \times (t - 655)}{\{1 + [-0.0073(t - 655)]^2\}^2}$$

The correlation coefficient for these results is 0.996, indicating a very high fitting precision. In the displacement curve (Fig. 6), the solid line represents the portion of the curve obtained from fitting of the measured data to Eq. (1). It records the ground deformation process at monitoring point G22. The inflection point of the curve $P_2 = 655$ occurred on September 23, 2012, when the settling velocity reached its maximum value. According to the overlying strata rock mass deformation characteristics in the various fracture zones, it can be deduced that a wide range of gob roof caving occurred before September 23, 2012. The dashed line in Fig. 6 represents the predicted settlement deformation trend of monitoring point G22. The asymptote of the curve corresponds to the maximum value of the cumulative settlement deformation; thus, the final settlement deformation value at monitoring point G22 is 31.09 cm. By the end of March 16, 2013, the

cumulative amount of settlement deformation of G22 is 28.26 cm. The subsidence reached 90.9 % of the total subsidence; therefore, the estimated remaining sinkage is 2.83 cm. Based on the sinking speed at the surface, the whole movement process of the ground subsidence can be divided into three stages: the beginning, active, and decline stages (Zhang and Chong 2012). Currently, the average speed of the ground subsidence deformation is 0.006 mm/d, and its sinking speed is <1.7 mm/d; these rates indicate that the ground subsidence deformation stage is in the declining stage. The subsidence curve tends to flatten, and the surface deformation tends to stabilize at this stage. Therefore, if the existing geological conditions in the Taihe coal mining area are maintained and the mining conditions remain unchanged, no control measures are required to prevent the ground collapse in the Taihe coal mining area. Thus, the high precision of this prediction model provides a reference for the evaluation and treatment of ground subsidence in the Taihe coal mining areas.

8 Conclusions

The deformation features of the ground subsidence caused by underground mining in the Taihe coal mining area are in accordance with “S”-shaped curve characteristics.

The application of the arc tangent function in the mining subsidence deformation shows very good medium- and short-term forecasting accuracy.

This model is a real-time forecasting model; based on the latest monitoring data, the latest fitting parameters and the most up-to-date fitting curve will be obtained. Through constant correction of the model parameters, the dynamic development trend of subsidence deformation in the mining area will be grasped and high-precision forecasting capabilities can be achieved.

This function model has certain scope of application. This model will gain a better prediction effect when the overlying strata in the mined-out area under the action of its self-weight and the upper load. However, when large-scale external geological agency occurs, like earthquake, tectonic movement, the deformation features of the ground subsidence will be not in accordance with “S”-shaped curve characteristics. In this condition, the prediction precision will be low, and the model will be not suitable.

Acknowledgments This project was financially supported by the Basic Research Foundation of Jilin University (Grant No.201103139). Special gratitude is also extended to those participants who have contributed to this work.

References

- Chengdong S, MingGu X, Guo W (2012) The study of the compaction characteristics of the broken rock of coal seam road. *J rock mech eng* 31(1):1140–1144
- Lee S, Park I, Choi J-K (2012) Spatial prediction of ground subsidence susceptibility using an artificial neural network. *Environ Manage* 49:347–358
- Levenberg K (1944) A method for the solution of certain non-linear problems in least squares. *Q Appl Math* 2(2):164–168
- Li G, Zhang H, Li H (2013) The comparative analysis of probability integration and numerical simulation in surface subsidence prediction. *Appl Mech Mater* 295–298:3015–3018
- Lourakis MIA (2005) A brief description of the Levenberg–Marquardt algorithm implemented by levmar. *Found Res Technol* 4:1–6

- Marquardt DW (1963) An algorithm for the least-squares estimation of nonlinear parameters. *J Soc Ind Appl Math* 11(2):431–441
- Nie L, Zhang M, Jian H (2013) Analysis of surface subsidence mechanism and regularity under the influence of seism and fault. *Nat Hazards* 66:773–780
- Saeidi A, Deck O, Al Heib M, Rouleau A (2013) Adjusting the influence function method for subsidence prediction. *Key Eng Mater* 553:59–66
- Wang J (2003) The analysis of the prediction of the landslide. *Chin J Geol Hazard Control* 14(2):1–8
- Williams S, Bock Y, Pang P (1998) Integrated satellite interferometry: tropospheric noise, GPS estimates and implications for interferometric synthetic aperture radar products. *Geophysics* 103(11):27051–27067
- Xu N, Kulatilake PHSW, Tian H, Wu X, Nan Y, Wei T (2013) Surface subsidence prediction for the WUTONG mine using a 3-D finite difference method. *Comput Geotech* 48:134–145
- Xu H, Liu B, Fang Z (2014) New grey prediction model and its application in forecasting land subsidence in coal mine. *Nat Hazards* 71:1181–1194
- XunChun W, Yue Z, XingGe J, Pengl Z (2011) A dynamic prediction method of deep mining subsidence combines d-insar technique. *Procedia Environ Sci* 10:2533–2539
- Zhang J, Chong L (2012) The discussion of the surface and building deformation in the coal mining subsidence area. *Shanxi Archit* 38(9):83–84
- Zhao J, Sun Z, Zhang Z, Liu T (2010) A brief analysis of the collapse mechanism and development factors of the multilayer goaf. *Gr Water* 32(2):158–161. doi:[10.3969/j.issn.1004-1184.2010.02.067](https://doi.org/10.3969/j.issn.1004-1184.2010.02.067)